

Ultrabroadband Biphotons Generated via Chirped Quasi-Phase-Matched Optical Parametric Down-Conversion

Magued B. Nasr,¹ Silvia Carrasco,¹ Bahaa E. A. Saleh,¹ Alexander V. Sergienko,¹ Malvin C. Teich,¹ Juan P. Torres,² Lluís Torner,² David S. Hum,³ and Martin M. Fejer³

¹*Quantum Imaging Laboratory**, Departments of Electrical & Computer Engineering and Physics, Boston University, Boston, Massachusetts 02215, USA

²*ICFO-Institut de Ciències Fòniques, and Department of Signal Theory and Communications, Universitat Politècnica de Catalunya, Mediterranean Technology Park, 08860 Castelldefels (Barcelona), Spain*

³*E. L. Ginzton Laboratory, Stanford University, Stanford, California 94305, USA*

(Received 12 December 2007; published 5 May 2008; publisher error corrected 6 May 2008)

We generate ultrabroadband biphotons via the process of spontaneous parametric down-conversion (SPDC) in quasi-phase-matched nonlinear gratings that have a linearly chirped wave vector. By using these ultrabroadband biphotons (300-nm bandwidth), we measure the narrowest Hong-Ou-Mandel dip to date, having a full width at half maximum of 7.1 fs. This enables the generation of a high flux of nonoverlapping biphotons with ultrabroad bandwidth, thereby promoting the use of SPDC light in many nonclassical applications.

DOI: [10.1103/PhysRevLett.100.183601](https://doi.org/10.1103/PhysRevLett.100.183601)

PACS numbers: 42.50.Dv, 42.65.Lm, 42.65.Re

One of the goals of quantum optics is to design and implement new sources of quantum light, such as entangled photons (*biphotons*), with tunable spectral properties that match the specific application under consideration. The most widely used method for the generation of biphotons is spontaneous parametric down-conversion (SPDC) [1,2], where two lower-frequency photons are generated when a strong pump field interacts with a nonlinear crystal.

As an example, the optimum biphoton bandwidth for atom-photon interactions associated with specific atomic transitions is ultranarrow (\sim MHz) [3], whereas it is ultrabroad for high-axial-resolution quantum optical coherence tomography (QOCT) [4]. Indeed, the generation of ultrabroadband SPDC can yield a high flux of nonoverlapping biphotons with optical powers in the microwatt region [5], which is essential for making use of SPDC light in nonclassical applications such as entangled-photon microscopy [6], spectroscopy [7], lithography [8], and photoemission [9].

By and large, ultrabroadband biphotons are not harvested directly at the output of a bulk down-converting crystal, unless it is extremely thin ($\sim 50 \mu\text{m}$), in which case the biphoton flux is very low [10]. Various other methods to generate such biphotons have been suggested and/or experimentally implemented [11–15]. One such method, which is of principal interest in this Letter, makes use of a quasi-phase-matched (QPM) nonlinear grating with a nonuniform poling period Λ [11]. The poling pattern $\Lambda(z)$, where z is the spatial coordinate along the direction of pump propagation, serves a twofold purpose: The first is to provide a collection of phase-matching conditions over the length of the grating, which leads to broadband biphoton generation. The second is to control the spread of the biphoton wave packet, i.e., the temporal separation between the signal and idler photons comprising a pair, which

is achieved by constraining the location at which a signal-idler wavelength pair is generated; this serves to tailor the phase relation between the various spectral components. For example, in the absence of group-velocity dispersion, a linearly chirped spatial frequency $K_g(z) = 2\pi/\Lambda(z)$ ensures an exact linear chirp of the biphoton wave packet [15], which is readily compressed by using the techniques of ultrafast optics [16].

In this Letter, by using appropriately designed QPM samples, we demonstrate the generation of ultrabroadband biphotons (around 300 nm), the largest ever, to the best of our knowledge. By using these biphotons, on the twentieth anniversary of the development of the Hong-Ou-Mandel (HOM) interferometer [17], we report the narrowest HOM dip measured to date, with a FWHM of 7.1 fs. This corresponds to an axial resolution of $1.1 \mu\text{m}$ in QOCT.

Theory.—For a monochromatic pump of angular frequency ω_p and noncollinear degenerate emission, the biphotons are characterized by the frequency-entangled state

$$|\psi\rangle = \int d\Omega \phi(\Omega) |\omega_0 + \Omega\rangle_s |\omega_0 - \Omega\rangle_i, \quad (1)$$

where Ω is the angular-frequency deviation about the degenerate angular frequency $\omega_0 = \omega_p/2$, the complex function $\phi(\Omega)$ is the biphoton spectral density, $|\phi(\Omega)|^2$ is the biphoton power spectral density, and each of the signal and idler photons resides in a single spatial mode, indicated by the subscripts s and i , respectively, in Eq. (1). For collinear emission, one can associate the signal (idler) photon with a wavelength below (above) the degeneracy point.

The SPDC source we consider is a QPM grating with a linearly varying spatial frequency given by $K_g(z) = K_0 - \alpha z$, where K_0 is the grating's spatial frequency at its

entrance face ($z = 0$) and α is a parameter that represents the degree of linear chirp. We make use of third-order QPM for which $K_g(z) = 3 \times 2\pi/\Lambda(z)$. By using a plane-wave approximation for the pump, signal, and idler and assuming that the value of the second-order susceptibility $\chi^{(2)}$ is wavelength-independent, we compute the biphoton spectral density to be $\phi(\Omega) \propto \int_0^L dz \exp\{j[\Delta k(\Omega) + (\alpha z/2)]z\}$, which turns out to be [18]

$$\phi(\Omega) \propto \exp\left[\frac{-j\Delta k^2(\Omega)}{2\alpha}\right] \left\{ \operatorname{erfi}\left[\frac{(1+j)\Delta k(\Omega)}{2\sqrt{\alpha}}\right] - \operatorname{erfi}\left[\frac{(1+j)[\Delta k(\Omega) + \alpha L]}{2\sqrt{\alpha}}\right] \right\}, \quad (2)$$

where $\Delta k(\Omega) = k_p(\omega_p) - k_s(\omega_0 - \Omega) \cos(\theta) - k_i(\omega_0 + \Omega) \cos(\theta) - K_0$ is the phase mismatch to all orders with no approximations; $k_q = \omega_q n_e(\omega_q, T)/c$, with $q = p, s, i$, is the amplitude of the wave vector for the pump, signal, and idler, respectively; θ is the angle between the signal (idler) direction and that of the pump; $j = \sqrt{-1}$; L is the length of the nonlinear grating; and erfi is the imaginary error function. The extraordinary refractive index $n_e(\omega_q, T)$ for the near-stoichiometric lithium tantalate (SLT) material used in our study can be computed by using a Sellmeier equation [19], where T is the temperature in degrees Celsius.

The measured photon rate at the output of a Michelson interferometer $I(\tau) \propto G_\tau^{(1)}(0)$ is given by

$$I(\tau) \propto \int d\Omega |\phi(\Omega)|^2 + \operatorname{Re}\left\{ e^{-j\omega_0\tau} \int d\Omega |\phi(\Omega)|^2 e^{-j\Omega\tau} \right\}, \quad (3)$$

where $G^{(1)}(t') = \langle \psi | E^{(-)}(t) E^{(+)}(t + t') | \psi \rangle$ is the first-order correlation function, which is independent of t for a stationary process [20]; $E^{(+)}$ and $E^{(-)}$ are the positive- and negative-frequency components of the electric field at the detector, respectively; and τ is the temporal delay between the two arms of the interferometer. The Fourier transform of $I(\tau)$ yields the biphoton power spectral density $|\phi(\Omega)|^2$.

In a HOM interferometer, the rate of coincidence between the electrical signal of two spatially separated *slow* single-photon detectors $N_c(\tau) = \int dt' G_\tau^{(2)}(t')$ is measured. Here τ is the relative delay between the signal and idler photons and $G^{(2)}(t') = \langle \psi | E^{(-)}(t) E^{(-)}(t + t') E^{(+)}(t + t') E^{(+)}(t) | \psi \rangle$ is the second-order correlation function, which is independent of t for a stationary process [20], so that

$$N_c(\tau) = \int d\Omega |\phi(\Omega)|^2 - \operatorname{Re}\left\{ \int d\Omega \phi(\Omega) \phi^*(-\Omega) e^{-2j\Omega\tau} \right\}. \quad (4)$$

Experiment—Our biphoton source, shown in Fig. 1(a), consists of an SLT crystal onto which six equal-length

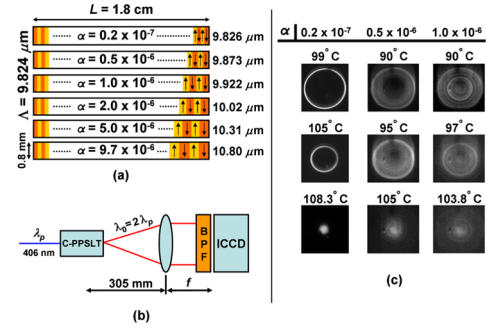


FIG. 1 (color online). (a) The C-PPSLT gratings with six different degrees of chirp α , specified in units of μm^{-2} . The poling period at the entrance face of each grating ($z = 0$) is fixed at $\Lambda = 9.824 \mu\text{m}$; the values at the exit face are indicated. For the grating with the lowest (highest) chirp, the poling period changes by about 0.02% (10%) over its length. (b) Setup used to image the emission-cone cross sections from the C-PPSLT gratings. A monochromatic Kr^+ -ion laser operated at $\lambda_p = 406 \text{ nm}$ pumps the C-PPSLT gratings. BPF represents a 10-nm bandpass filter at the degenerate wavelength $\lambda_0 = 812 \text{ nm}$, and ICCD represents an intensified charge-coupled device camera, which is placed in the Fourier plane of an $f = 100\text{-mm}$ lens. (c) The emission-cone cross sections from C-PPSLT gratings at the degenerate wavelength at different temperatures, for various values of the chirp parameter α .

($L = 1.8 \text{ cm}$) gratings have been poled with a linearly chirped spatial frequency, with various degrees of chirp α . Our SLT was fabricated from congruently melting composition lithium tantalate by using the vapor-transport-equilibration (VTE) method [21].

We first study the spatial distribution of degenerate SPDC emission by using the experimental arrangement depicted in Fig. 1(b). The results are displayed in Fig. 1(c), where we show intensified charge-coupled device camera (ICCD) images of the SPDC emission-cone cross sections at different temperatures, for different chirped periodically poled stoichiometric lithium tantalate (C-PPSLT) gratings. For a weakly chirped grating ($\alpha = 0.2 \times 10^{-7} \mu\text{m}^{-2}$), the observation of a well-defined ring of emission, showing a transition from noncollinear to collinear behavior as the temperature increases, indicates that the direction of emission is strongly determined by the wavelength of observation, which is fixed by the bandpass filter (BPF). It is worth noting that the experimental temperature that led to collinear degenerate emission ($T = 108.3^\circ\text{C}$) was larger than that calculated from the Sellmeier equation for SLT grown by using the double-crucible Czochralski (DCC) method [19] ($T = 60^\circ\text{C}$). This discrepancy is most likely explained by a $0.1\text{-}\mu\text{m}$ period fabrication error; however, it may also stem from the differences in stoichiometry between SLT fabricated by the VTE and DCC methods. As the degree of chirp is increased, the emission cross section takes the form of a hollow disk ($\alpha = 0.5 \times 10^{-6} \mu\text{m}^{-2}$), which then be-

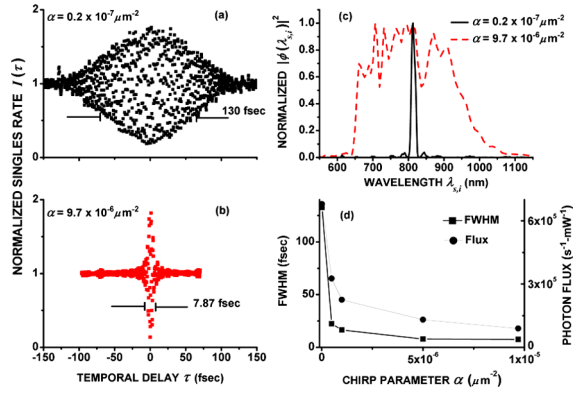


FIG. 2 (color online). Normalized interferogram $I(\tau)$ for collinear SPDC. Emission from a C-PPLT grating with (a) $\alpha = 0.2 \times 10^{-7} \mu\text{m}^{-2}$ exhibits a FWHM of 130 fs and (b) $\alpha = 9.7 \times 10^{-6} \mu\text{m}^{-2}$ exhibits a FWHM of 7.87 fs. (c) The power spectral densities $|\phi(\Omega)|^2$, plotted vs wavelength $\lambda_{s,i}$, for the data shown in (a) and (b). (d) The FWHM (squares) of the measured interferograms for gratings of different degrees of chirp are plotted on the left ordinate. The biphoton fluxes per milliwatt of pump power (circles) are plotted on the right ordinate. The lines connecting the experimental points are for guiding the eye.

comes a full disk with further increase ($\alpha = 1 \times 10^{-6} \mu\text{m}^{-2}$). This implies that, for a given wavelength, more emission directions are possible as the chirp increases.

For a fixed direction, increased chirping is expected to lead to a broader spectrum [15]. We demonstrate this by measuring the interferogram of collinear SPDC emission $I(\tau)$ by using a Michelson interferometer. The results are shown in Fig. 2. In Fig. 2(a), for the lowest-chirped grating ($\alpha = 0.2 \times 10^{-7} \mu\text{m}^{-2}$), the interferogram exhibits a FWHM of 130 fs at $T = 108.3^\circ\text{C}$, whereas in Fig. 2(b), for the highest-chirped grating ($\alpha = 9.7 \times 10^{-6} \mu\text{m}^{-2}$), the FWHM is 7.87 fs at $T = 45.4^\circ\text{C}$. The corresponding power spectral densities, obtained from the Fourier transform of the measured interferograms in accordance with Eq. (3), are presented in Fig. 2(c). The emission from the highest-chirped grating exhibits an ultrabroadband power spectral density $|\phi(\Omega)|^2$ (plotted vs $\lambda_{s,i}$, rather than vs Ω , for clarity) that spans approximately 300 nm about the degenerate wavelength $\lambda_0 = 812$ nm. This salutary spectral broadening is accompanied by a decrease in the biphoton flux, as shown in Fig. 2(d). As the chirp is increased, the total number of down-converted biphotons is redistributed over a broader range of emission angles and over a broader spectrum, as is evident in Figs. 1(c) and 2(c), respectively, thereby reducing the biphoton flux for a fixed experimental collection angle.

Finally, we demonstrate the ultranarrow dip that can be attained by using these biphotons when they are employed in a HOM interferometer [17]. The normalized coincidence rates $N_c(\tau)$ are depicted in Fig. 3 for biphotons

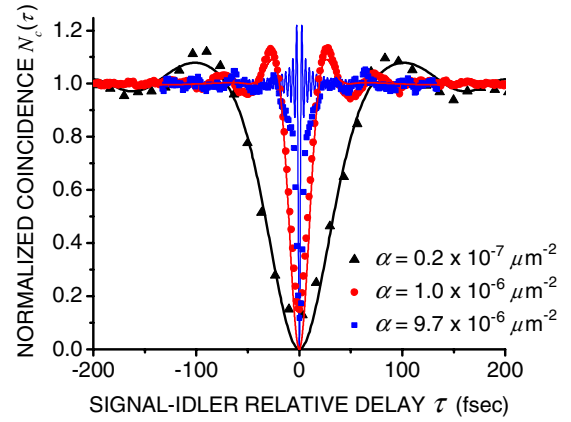


FIG. 3 (color online). Normalized HOM coincidence interferograms (dips) for various values of the chirp parameter α . The symbols represent the measured data points, whereas the solid curves are the corresponding numerical simulations using Eqs. (2) and (4). The FWHM of the measured dips are 77, 19.1, and 7.16 fs for $\alpha = 0.2 \times 10^{-7}$, 1.0×10^{-6} , and $9.7 \times 10^{-6} \mu\text{m}^{-2}$, respectively.

generated by C-PPLT gratings with $\alpha = 0.2 \times 10^{-7}$ at $T = 106.5^\circ\text{C}$, $\alpha = 1.0 \times 10^{-6}$ at $T = 76.5^\circ\text{C}$, and $\alpha = 9.7 \times 10^{-6} \mu\text{m}^{-2}$ at $T = 52.6^\circ\text{C}$. All of these experiments were conducted at a noncollinear emission angle of $\theta \approx 1.1^\circ$. The effect of chirping is clearly evident, as the HOM dip narrows from a FWHM of 77 fs for a weakly chirped grating to 7.16 fs for the highest-chirped grating. This observed narrow dip translates to an ultrahigh axial resolution of $1.1 \mu\text{m}$ in a QOCT experiment. We should point out that the semiconductor single-photon avalanche photodiodes that have been used in our experiments (EG&G-SPCM-AQR-15) have a limited bandwidth, particularly in the near infrared region. An even narrower HOM dip would emerge, were we to make use of broader bandwidth devices, such as superconducting single-photon detectors [22].

Discussion — Our observation of an ultranarrow HOM dip indicates that the spectral density of the observed biphotons is ultrabroad. However, this does not necessarily mean that the biphoton entanglement time is ultranarrow. While the entanglement time is the width of the biphoton wave packet $f(\tau)$, which is the inverse Fourier transform of the biphoton spectral density $\phi(\Omega)$, the profile of the HOM dip is the inverse Fourier transform of the product $\phi(\Omega)\phi^*(-\Omega)$, which is insensitive to even-order components of the phase of $\phi(\Omega)$ [23], a nonclassical feature that is exploited in QOCT. The width of the HOM dip, in contrast, would give the narrowest value in time that a biphoton wave packet can attain, if all of the even phase terms were canceled.

The width of the biphoton wave packet may be observed by direct measurement of the second-order correlation function $G_\tau^{(2)}(t')$. This can be accomplished via a sum-frequency generation (SFG) experiment whereby a relative

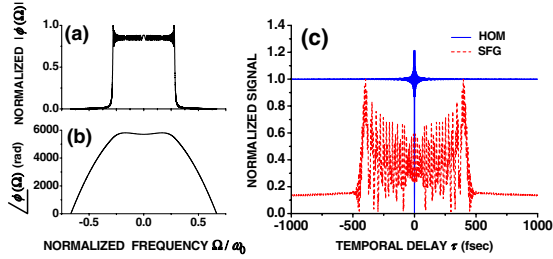


FIG. 4 (color online). (a) Magnitude and (b) phase of the biphoton spectral density $\phi(\Omega)$ as provided by Eq. (2), for $\alpha = 9.7 \times 10^{-6} \mu\text{m}^{-2}$. (c) Numerical simulation of the expected signal if these biphotons were employed in a HOM interferometer (solid blue curve) or in an SFG experiment (dashed red curve). The outcome of an SFG experiment is a direct measure of the biphoton wave packet square magnitude $|f(\tau)|^2$.

temporal delay τ is introduced between the signal and idler photons, which are focused onto a second-order nonlinear crystal that serves as a fast autocorrelator. The SFG rate $S(\tau)$, which is proportional to the coincident spatial and temporal arrivals of the two photons, i.e., to $G_{\tau}^{(2)}(0)$, is given by $S(\tau) \propto |\int d\Omega \phi(\Omega) \exp(-j\Omega\tau)|^2 = |f(\tau)|^2$.

The biphotons that were employed in our experiments were far from being transform-limited. To demonstrate this, we plot in Figs. 4(a) and 4(b), respectively, the magnitude and phase of $\phi(\Omega)$ provided in Eq. (2), for $\alpha = 9.7 \times 10^{-6} \mu\text{m}^{-2}$ at $T = 52.6^\circ\text{C}$. In Fig. 4(c), we present a numerical simulation of the HOM profile (solid blue curve) and the biphoton wave packet square magnitude $S(\tau) \propto |f(\tau)|^2$ (dashed red curve), as it would be obtained in an SFG experiment, which is more than 2 orders of magnitude wider than the HOM profile. This significant temporal spread is attributable to the phase of $\phi(\Omega)$. If this phase were to be eliminated by use of an appropriate phase filter [5], the biphoton wave packet would be compressed to its transform-limited width.

Finally, we provide an important example of how the results provided in this Letter can be used to advance our understanding of the interaction of entangled light with matter. Despite numerous attempts, the phenomenon of entangled-photon photoemission [9] has not been experimentally observed. Careful analysis reveals that the entangled-photon photocurrent i_e decreases with increasing entanglement time T_e . In particular, for degenerate photons impinging on the bialkali material K_2CsSb , i_e is calculated to be a factor of 10 greater than the semiclassical two-photon photocurrent when $T_e = 7$ fs (they are roughly equal when $T_e = 40$ fs) [9]. The results reported in this Letter should therefore make entangled-photon photoemission observable for the first time.

This work was supported by a U.S. Army Research Office (ARO) Multidisciplinary University Research

Initiative (MURI) grant; by the Bernard M. Gordon Center for Subsurface Sensing and Imaging Systems (CenSSIS), an NSF Engineering Research Center; by the Intelligence Advanced Research Projects Activity (IARPA) and ARO through Grant No. W911NF-07-1-0629; by the European Commission (QAP, IST directorate, Contract No. 015848); and by the Government of Spain (Consolider Ingenio 2010 QIOT No. CSD2006-00019 and No. FIS2007-60179). We are most grateful to S. E. Harris and M. Saleh for valuable discussions.

*<http://www.bu.edu/qil>

- [1] S. E. Harris, M. K. Oshman, and R. L. Byer, Phys. Rev. Lett. **18**, 732 (1967); R. L. Byer and S. E. Harris, Phys. Rev. **168**, 1064 (1968).
- [2] D. Magde and H. Mahr, Phys. Rev. Lett. **18**, 905 (1967); D. N. Klyshko and D. P. Krindach, Zh. Eksp. Teor. Fiz. **54**, 697 (1968) [Sov. Phys. JETP **27**, 371 (1968)].
- [3] J. S. Neergaard-Nielsen *et al.*, Opt. Express **15**, 7940 (2007).
- [4] A. F. Abouraddy *et al.*, Phys. Rev. A **65**, 053817 (2002); M. B. Nasr *et al.*, Opt. Express **12**, 1353 (2004).
- [5] A. Pe'er *et al.*, Phys. Rev. Lett. **94**, 073601 (2005).
- [6] M. C. Teich and B. E. A. Saleh, Cesk. Cas. Fys. **47**, 3 (1997); U.S. Patent No. 5 796 477 (1998).
- [7] B. E. A. Saleh *et al.*, Phys. Rev. Lett. **80**, 3483 (1998).
- [8] A. N. Boto *et al.*, Phys. Rev. Lett. **85**, 2733 (2000).
- [9] F. Lissandrin *et al.*, Phys. Rev. B **69**, 165317 (2004).
- [10] E. Dauler *et al.*, J. Res. Natl. Inst. Stand. Technol. **104**, 1 (1999).
- [11] S. Carrasco *et al.*, Opt. Lett. **29**, 2429 (2004).
- [12] S. Carrasco *et al.*, Phys. Rev. A **70**, 043817 (2004); Phys. Rev. A **73**, 063802 (2006); Opt. Lett. **31**, 253 (2006).
- [13] M. B. Nasr *et al.*, Opt. Commun. **246**, 521 (2005).
- [14] K. A. O'Donnell and A. B. U'Ren, Opt. Lett. **32**, 817 (2007).
- [15] S. E. Harris, Phys. Rev. Lett. **98**, 063602 (2007); S. E. Harris and S. Sensarn, in *Proceedings of the Ninth Rochester Conference on Coherence and Quantum Optics (CQ09)* (OSA, Washington, DC, 2007), paper CMD1.
- [16] B. E. A. Saleh and M. C. Teich, *Fundamentals of Photonics* (Wiley, Hoboken, 2007), 2nd ed., Chap. 22.
- [17] C. K. Hong, Z. Y. Ou, and L. Mandel, Phys. Rev. Lett. **59**, 2044 (1987).
- [18] <http://integrals.wolfram.com/index.jsp>
- [19] A. Bruner *et al.*, Opt. Lett. **28**, 194 (2003).
- [20] R. J. Glauber, Phys. Rev. **130**, 2529 (1963).
- [21] M. Katz *et al.*, Opt. Lett. **29**, 1775 (2004); D. S. Hum *et al.*, J. Appl. Phys. **101**, 093108 (2007).
- [22] R. Sobolewski *et al.*, IEEE Trans. Appl. Supercond. **13**, 1151 (2003).
- [23] A. M. Steinberg *et al.*, Phys. Rev. A **45**, 6659 (1992); Phys. Rev. Lett. **68**, 2421 (1992).